Received: 9 June 2020 | Revised: 13 August 2020 | Accepted: 18 August 2020

DOI: 10.1002/app.49869

ARTICLE

Applied Polymer SCIENCE WILEY

# Observation of latent ion tracks in semicrystalline polymers by scanning electron microscopy

Irina V. Blonskaya[1] | Olga V. Kristavchuk[1] | Alexandr N. Nechaev[1,2] | Oleg L. Orelovich[1] | Olga A. Polezhaeva[1] | Pavel Y. Apel[1,2]

[1]Flerov Laboratory of Nuclear Reactions, Joint Institute for Nuclear Research, Dubna, Russia

[2]Dubna State University, Dubna, Russia

**Correspondence**
Pavel Y. Apel, Flerov Laboratory of Nuclear Reactions, Joint Institute for Nuclear Research, Dubna 141980, Russia.
Email: apel@jinr.ru

**Abstract**

Advances in nanotechnology and materials science require further improvement of metrology of nanostructured polymers, in particular, polymers modified by high energy ion beams. The observation of latent ion tracks using various microscopy methods is an important part of studies on heavy ion effects in solids. However, scanning electron microscopy (SEM) has not been utilized for polymers. In the present study, it is shown how SEM can be used to observe latent tracks in semicrystalline polymers. The procedure includes the embrittlement of a polymer specimen by controlled photooxidation and its subsequent fracture. Latent tracks are clearly visible on fractured surfaces as structureless stripes surrounded by an inhomogeneous semicrystalline matrix. Using this method, the latent tracks of Kr, Xe, Au, and Bi ions with energies of 1–11 MeV/u in polyethylene terephthalate and polypropylene films are observed and their diameters are estimated. In contrast to transmission electron microscopy, the suggested novel technique detects the outer track shell consisting of an amorphized polymer. Therefore, SEM observations can complement other commonly used techniques to comprehensively characterize the structure of ion tracks in polymers.

## 1 | INTRODUCTION

Ionizing radiation, including beams of accelerated ions, has been widely applied in modifying the structure and properties of polymers.[1,2] Swift heavy ions (SHI)—a form of particle radiation—have sufficient energy and mass to penetrate solids in a straight line and produce a continuous damage trail, called a latent track.[2,3] Over the last 60 years, the ability of SHI to produce latent tracks has become the reason for extensive fundamental and applied research works.[3] Both the mechanisms of track formation and the numerous applications in fields such as material science, nanotechnology, biophysics, and cosmic ray simulations have attracted the attention of the scientific community.

The observation of ion latent tracks using various microscopy methods is an important part of the studies on fundamental mechanisms of the SHI radiation effects. There are also technological advances that require detailed knowledge of the structure of the latent track in polymers. These are the fabrication of nanopore track-etched membranes, anisotropic ion-exchange membranes, membranes produced by the so-called "track-UV technique" and other functional nanomaterials.[4–9] Transmission electron microscopy (TEM) and scanning probe microscopy (SPM) have been widely employed to view ion tracks in solids. In the case of crystalline materials, TEM gives atomic-scale information on the damage as an amorphous region with sharp boundaries. In many inorganic materials such as oxides, the tracks consist of

  

amorphous cylinders imbedded in the crystalline matrix. Sometimes the track structure is more complex and consists of an amorphous core surrounded by a disordered crystalline shell.[3] Methodologically, TEM requires great effort in sample preparation and the success largely depends on the sample quality. Small angle scattering of X-rays and neutrons (SAXS and SANS, respectively) provides valuable data on the size and density deficit in latent tracks in different matrices, including polymers.[3,10–13]

Sophisticated TEM investigations yielded estimates of 6–10 nm for the diameter of a central track region of ion tracks in polyethylene (PE), polyethylene terephthalate (PET), and polyimide (PI).[14–17] Both TEM and small angle scattering characterize the ion track in polymers as a zone with a lower gravimetric density, that is, the zone that is called the "track core." At the same time, the ion tracks in polymer have an outer shell, the so-called "halo," where the density deficit is negligible but the chemical properties are modified. The halo forms due to secondary electrons and mobile radiolysis products at radial distances considerably exceeding the track core radius and can be detected using chemical etching. In case the cross-linking is the dominant process in the halo, the etching rate outside the track core is lower than the etching rate of pristine polymer.[4,18–20] To date, the latent track halo has not been measurable by means of any microscopy method. The existence of the halo manifests itself in the spatial distribution of monomer grafting onto ion-irradiated polymer foils[5,7,8] and in the shape of etched nanopores.[6,20] SPM images of latent tracks of SHI on the surface of polymer foils reveal ring-shaped structures, craters, and hillocks that can be associated with track halos.[21–23] However, these features reflect the interaction of an ion with the surface layer and do not directly relate to processes in bulk.

In contrast to TEM, scanning electron microscopy (SEM) has never been effective in studies of latent track morphology. To our knowledge, there have been no published reports on successful attempts to capture the image of latent tracks in polymers using SEM. The only relevant objects that have been viewed are the cross linked needle-like rods and nanowires obtained after the dissolution of irradiated material.[24,25] In this work, a preparation technique is proposed that makes latent tracks visible under SEM and the observed results of latent tracks in two semicrystalline polymers are presented. Both chosen polymers—polyethylene terephthalate and polypropylene (PP)—are of significant practical importance in modern technologies.

## 2 | EXPERIMENTAL

### 2.1 | Polymer foils and ion irradiation

Biaxially oriented semicrystalline foils of polyethylene terephthalate (12-μm-thick Hostaphan RNK, Mitsubishi Polyester Films, and 10-μm-thick foil GOST 24234-80, USSR production), and PP (10-μm-thick Torayfan T2372, Toray, Japan) were used. The degree of crystallinity of the PET foils, estimated by the X-ray diffraction method, was ~40%.[26] For the PP foils, this parameter was ~70% as deduced from the measured gravimetrical density of 0.91 g $cm^{-3}$.[27] Samples of polymer foils were irradiated with scanned beams of Xe ions at the IC-100 cyclotron and Bi and Kr ions at the U-400 cyclotron (FLNR JINR, Dubna). PP samples were irradiated with Au ions at the UNILAC facility of GSI (Darmstadt). The ion fluences varied from $3{\cdot}10^9$ to $3{\cdot}10^{11}$ $cm^{-2}$. All irradiations were performed perpendicular to foil surface in vacuum. The energy and the energy loss of the ions are summarized in Table 1. For simplicity, the energy loss data are presented as calculated by the SRIM computer code,[28] without correction. In reality, the $dE/dx$ values are larger by at least 10% because the code underestimates the energy losses of SHI with large atomic numbers in light targets such as polymers.[18]

### 2.2 | Preparation of samples and SEM investigation

All ion-irradiated PET samples were exposed to soft ultraviolet (UV) radiation of LE-30 lamps (Lisma, Saransk, Russia) in air using a pristine 12-μm-thick PET foil as filter, which was periodically replaced with a fresh piece of foil. The intensity of the UV radiation at the sample surface was 3–4 W $m^{-2}$ in the UVA range (315–400 nm) and ~1 W $m^{-2}$ in the UVB range (280–315 nm), as measured by a UV radiometer TKA-PKM (model 12, Russia). Nonfiltered radiation had approximately equal intensities in both UV ranges, 3–4 W $m^{-2}$. The suppression of the radiation with a wavelength of ≤315 nm provided nonaggressive conditions under which polymer samples undergo a slow photodegradation. As a result, the sample became very brittle and broke easily when touched with tweezers. The UV exposure needed to achieve satisfactory brittleness depends on the ion fluence. PET samples irradiated with fluences of $3{\cdot}10^{11}$ $cm^{-2}$ and $3{\cdot}10^9$ $cm^{-2}$ require a UV exposure of approximately 100 and 1,000 h, respectively. Samples of PP degraded several times faster than PET. The fractured samples were sputter-coated with a 10-nm-thick Au-Pd layer and examined with field

**TABLE 1** Atomic number, atomic mass, kinetic energy, and specific energy loss of ions used to produce tracks in polymer foils

| Ion, target | Atomic number | Atomic mass, a.m.u. | Kinetic energy, MeV | $dE/dx$[a], keV/nm | |
|---|---|---|---|---|---|
| Bi, 12 μm PET | 83 | 209 | 710 | 17.5 | 17.4 |
| Au, 10 μm PET | 79 | 197 | 2250 | 14.4 | 14.6 |
| Au, 10 μm PP | 79 | 197 | 2250 | 10.9 | 11.0 |
| Xe, 12 μm PET | 54 | 132 | 160 | 11.6 | 6.7 |
| Kr, 10 μm PET | 36 | 84 | 210 | 7.4 | 7.6 |

[a]Energy losses at the entrance and at the exit of the foils.

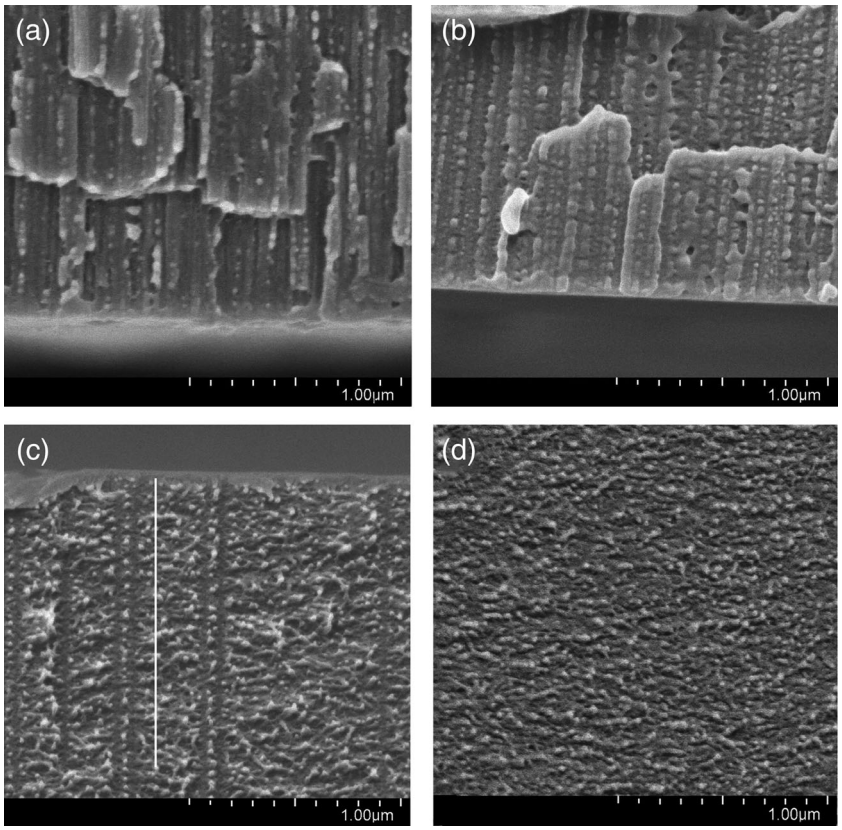


**FIGURE 1** Fractures of PET samples (Hostaphan RNK12), irradiated with Xe ions at fluences of of $3{\cdot}10^{11}$ cm$^{-2}$ (a), $3{\cdot}10^{10}$ cm$^{-2}$ (b), and $3{\cdot}10^{9}$ cm$^{-2}$ (c). The white vertical line in image (c) has a width of 10 nm. Micrograph (c) shows the layer where $dE/dx = 11.6$ keV/nm. Image (d): sample not exposed to heavy ions

emission microscopy (FESEM) using a Hitachi SU8020 instrument (Japan).

## 2.3 | UV and FTIR spectroscopy

Infrared spectra with a resolution of 2 cm$^{-1}$ were measured in external reflection at an angle of 42° on a Nicolet 6700 Fourier transform IR spectrometer (Thermo Scientific) by a Smart iTR™ Attenuated Total Reflectance sampling accessory equipped with a ZnSe crystal. Pristine PET samples as well as ion-irradiated and UV-exposed (after ion irradiation) PET samples were all examined in a wavenumber range where spectral peaks typical of crystalline and amorphous phases are present.[29] Ultraviolet absorption spectra were recorded on an Evolution 600 spectrophotometer (Thermo Scientific).

# 3 | RESULTS AND DISCUSSION

Figure 1 shows a series of FESEM images of fractured PET samples irradiated with different Xe ion doses and subjected to UV-embrittlement. For the highest ion fluence, $3{\cdot}10^{11}$ cm$^{-2}$, we clearly see a highly anisotropic relief of the fractured surface. No individual tracks can be identified. For the lowest ion fluence, $3{\cdot}10^{9}$ cm$^{-2}$, individual latent tracks are seen as homogeneous gray stripes surrounded by a polymer matrix consisting of alternating bright and dark grains. The bright grains, ranging from

5 to 20 nm in size, are crystallites or crystalline nanofibrils typical of biaxially oriented PET foils.[30–33] More than 50% of the polymer volume is comprised of the amorphous phase, which appears as the structureless background between the crystallites (see Figure 1d for a sample not irradiated with ions). Individual latent tracks are visible in Figure 1c because the ions destroy crystallites along their trajectories, and the damage zones look similar to the pristine amorphous material. Due to a high fluence, the tracks overlap in Figure 1a, and there are almost no crystallites seen on the fractured surface. An intermediate situation is shown in Figure 1b where crystallites occupy a considerable fraction of the imaged cross section.

Figure 2 is another illustration of the combined action of ion irradiation and UV exposure on a PET foil. The electron micrograph in Figure 2a shows a sample that has been irradiated with Au ions and then exposed to nonfiltered UV radiation for 200 h. Photooxidation with a more energetic UV radiation leads to a rapid degradation of the polymer and at the same time destroys the crystalline phase. The fractured surface is more or less homogeneous and ion tracks are not revealed. In contrast, a sample of the same foil that has been exposed to filtered UV, shows both clear ion tracks and semicrystalline morphology of the matrix not damaged by ions (Figure 2b).

In order to better understand the essence of the observed phenomena, we employed Fourier transform infrared spectroscopy. IR spectra of PET contain bands reliably assigned to certain chain conformations in crystalline and amorphous phases, which allows the estimation of the changes in crystallinity under either ion or UV irradiation. Based on the data from literature, band intensities at wavenumbers of 1,370.9 and 1,470.8 $cm^{-1}$ were used as the measures of the degree of crystallinity.[29] The former corresponds to the $CH_2$ wagging mode of gauche conformation of ethylene glycol moiety in the amorphous phase. The latter is the $CH_2$ bending mode of trans glycol conformation which exists in two different polymer repeat units. One is the true crystalline form, called TC, in which both the glycol and terephthaloyl moieties are in an "all trans" arrangement.[29] The other is the unit where the glycol moiety is in the trans conformation but the terephthaloyl conformation remains rather disordered. This arrangement, called TX, is typical of stretched PET. Therefore, an increase in intensity of the 1,370 $cm^{-1}$ band and a decrease in intensity of the 1,470 $cm^{-1}$ band should indicate amorphization of the polymer. However, the 1470/1370 band intensity ratio will not tend to zero because of the presence of the TX structure. Figure 3a,b shows the change in the 1470/1370 band intensity ratio depending on ion fluence and UV exposure. The ratio monotonically decreases with increasing ion fluence, thus showing effective amorphization of the crystalline fraction of the polymer. This phenomenon takes place under the SHI irradiation of many polymers, including PET.[26,34–36] The effect of soft UV radiation is different. A several percent drop in the apparent crystallinity is observed after 1 h of UV exposure and practically no changes occur for further exposures as long as ~100 h and even ~1,000 h (see point B in Figure 3b). Assumingly, the rapid changes in the beginning of the UV treatment are related to transformations in a metastable phase of PET. A strong decrease in the mechanical strength and elasticity of the PET samples indicates that the polymer undergoes photodegradation. At the same time its crystallinity stays constant which inevitably leads to the conclusion that the degradation occurs merely in the amorphous phase. This is the key condition for the successful observation of latent tracks on the fractured surfaces.

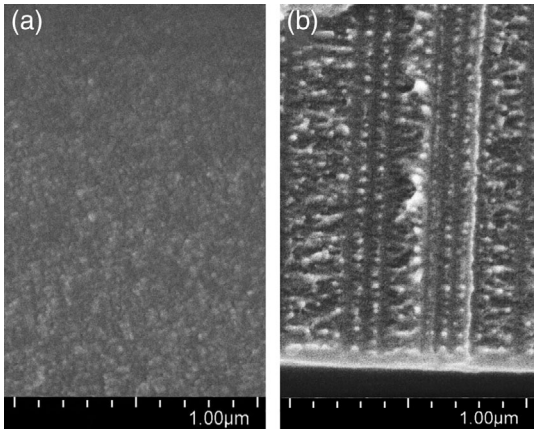


**FIGURE 2** Polyethylene terephthalate (PET) sample of a 10-μm thickness irradiated with Au ions ($8{\cdot}10^9$ $cm^{-2}$) after a 200 h exposure to non-filtered UV radiation (a) and after a 2,000 h exposure to filtered UV radiation (b)

Data in Figure 3b illustrate how the UV exposure needed to obtain good fractures depends on ion fluence. In point A, at the ion fluence of $3{\cdot}10^{11}$ $cm^{-2}$, the ions greatly contributed to the degradation of the polymer, and a UV exposure of 120 h was enough to make the sample brittle. In point B, at the ion fluence of $3{\cdot}10^{10}$ $cm^{-2}$, the degradation induced by ions was much weaker and, thus, a one order of magnitude longer UV exposure was required to destroy the sample.

It should be noted that the chance to obtain good images of the latent tracks depends on quite subtle differences in the preparation procedure. The UV exposure should be adjusted precisely and the method of trial and error is inevitable when working with a specific sample of PET. Though a soft UV spectrum is used, the UV

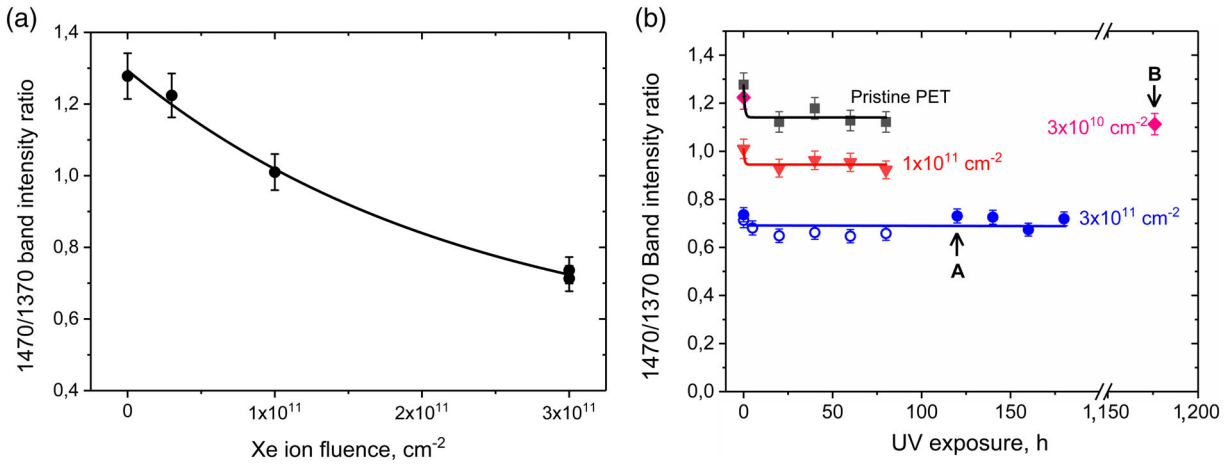


**FIGURE 3** The 1,470 to 1,370 $cm^{-1}$ band intensity ratio as a function of ion fluence (a) and exposure to filtered UV radiation (b). In panel (b), pristine polyethylene terephthalate (PET) foil Hostapahan RNK12 (squares), PET irradiated with Xe ion fluences of $3{\cdot}10^{10}$ $cm^{-2}$ (rhombs), $1{\cdot}10^{11}$ $cm^{-2}$ (triangles), $3{\cdot}10^{11}$ $cm^{-2}$ (circles). Open and solid circles show the results of two different series of experiments. Points A and B indicate the moments when samples of Figure 1a,b became brittle enough to be fractured. Error bars are sample standard deviations [Color figure can be viewed at wileyonlinelibrary.com]

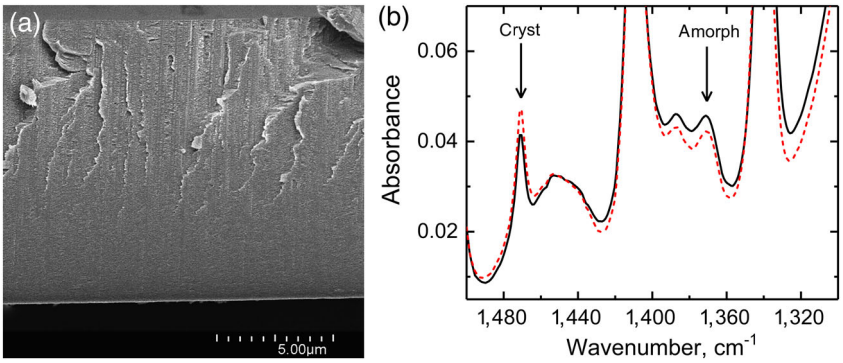


**FIGURE 4** (a) FESEM image of a polyethylene terephthalate (PET) sample Hostaphan RNK12 irradiated with Bi ions ($3{\cdot}10^{9}$ $cm^{-2}$) and exposed to UV radiation for 2,000 h. (b) FTIR spectra recorded on bottom (solid line) and top (dashed line) sides of the sample. Arrows point to a "crystalline" (1,470 $cm^{-1}$) and an "amorphous" (1,370 $cm^{-1}$) band. Note that d$E$/d$x$ is nearly constant across the foil (see Table 1) [Color figure can be viewed at wileyonlinelibrary.com]

radiation partially absorbs in the PET foil. Therefore, the rate of photooxidation is not constant across the foil. Figure 4a shows a sample that received a very high dose of UV radiation from the bottom. The 1470/1370 band intensity ratio was calculated from spectra for both sides of the foil (Figure 4b). Its value of 1.11 for the top side of the foil reflects the favorable situation for imaging the ion tracks. The polymer retained a sufficient degree of crystallinity in the upper half of foil thickness where ion tracks are seen. In contrast, the tracks were "erased" in the bottom layers of the foil which were overexposed and where the band intensity ratio decreased down to 0.96. A moderate reduction in crystallinity deteriorated the contrast between pristine matrix and ion tracks. Most probably, the admixture of the UVB range (~1 W $m^{-2}$) in the filtered UV radiation is responsible for this effect. Electromagnetic quanta of a higher energy strongly reduce the crystallinity. The 1470/1370 band intensity ratio for the sample shown in Figure 2a was estimated to be 0.73 (on the side that faced the UV lamp).

The reason why the photooxidation under soft UV radiation occurs predominately in amorphous PET while a more energetic radiation destroys the crystallites is not quite clear. Both long-wave and short-wave UV radiations were shown to induce photochemical degradation of PET, though at considerably different rates.[37] It is known that oxygen dissolves in amorphous regions of PET and does not penetrate the crystalline phase.[38–40] One can speculate that electromagnetic quanta of lower energy can induce chain ruptures only in the presence of oxygen while more energetic quanta induce direct chain scissions. Water, dissolved in the amorphous domains, can also facilitate heterogeneous degradation[38,41] and therefore the influence of moisture should not be ruled out and can be a subject of further research. Note also that commercial PET foils always contain organic and

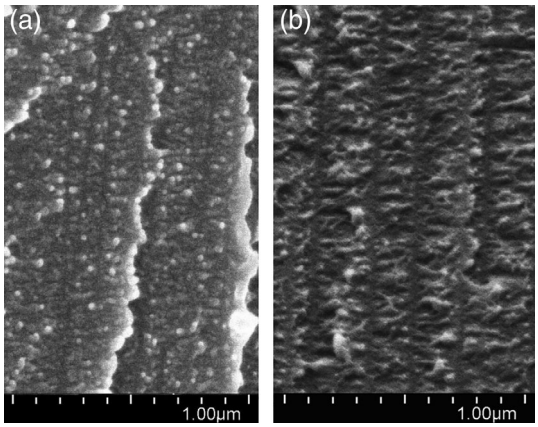


**FIGURE 5** Latent tracks of Kr (a) and Bi (b) ions in polyethylene terephthalate (PET) samples of a 10 μm and a 12 μm thickness, respectively

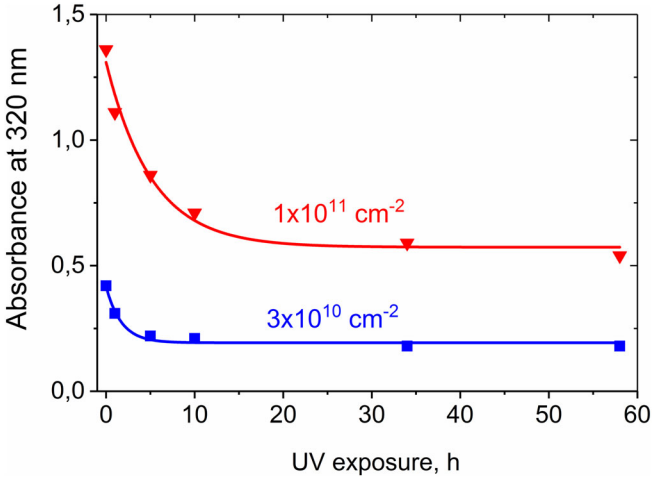


**FIGURE 6** Decrease in the absorbance of PET films Hostaphan RNK12 irradiated with xenon ions as a function of UV exposure time. Curves 1 and 2 correspond to ion fluences of $3 \times 10^{10}$ and $1 \times 10^{11}$ cm$^{-2}$, respectively. Optical absorption was measured at a wavelength of 320 nm [Color figure can be viewed at wileyonlinelibrary.com]

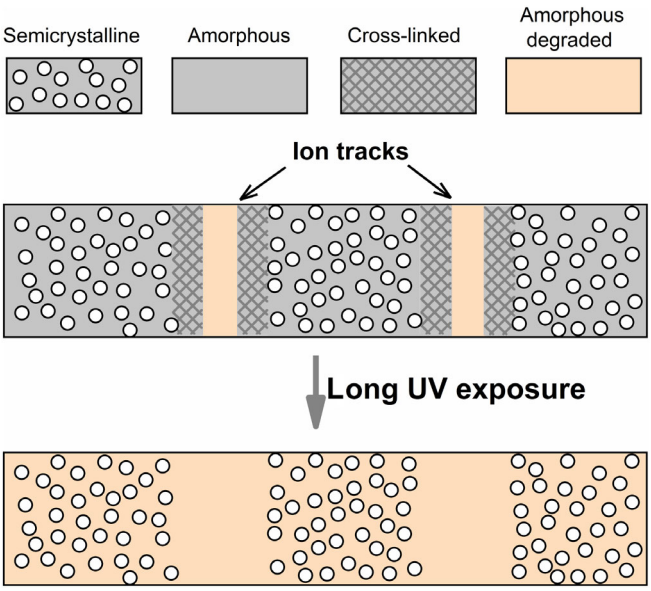


**FIGURE 7** Transformations in ion-irradiated polyethylene terephthalate (PET) for visualization of latent tracks in FESEM [Color figure can be viewed at wileyonlinelibrary.com]

inorganic additives which make photochemical processes rather complicated.[42]

Direct observations of latent ion tracks often aim at studying the relationship between the track morphology and the electronic energy loss, d$E$/d$x$, of the bombarding particles.[3] The images obtained in the present study allow one to give some preliminary comments regarding this aspect. Figures 1c, 2b, and 5b show the tracks of ions with increasing energy losses—Xe, Au, and Bi—at nearly the same magnification. The tracks look very similar and it is difficult to find a quantitative difference in track characteristics such as track width. However, tracks of the lightest ion, Kr, look completely different (Figure 5a). The Kr ion tracks are much thinner (~10 nm) and sometimes poorly distinguishable on the rough fracture surface. Thus, our data for the ions with different atomic numbers show a tendency which is typical of the track radius versus energy loss dependence, that is, with a sharp increase at lower d$E$/d$x$ and a moderate slope at higher d$E$/d$x$.[3,18] The apparent radius of the Xe, Au, and Bi tracks in the SEM images is approximately 15–20 nm. This value correlates well with the radius of the track halo found in the etching experiments with single tracks of ions with high atomic numbers in similar PET foils.[20] However, our data do not constitute a regular dependence of the track width on the energy loss. Apparently, tracks of different ions in the same foil, with the same ion fluence, and subjected to identical preparation procedure should be employed to have a chance for a quantitative comparison. This systematic set of images should be treated using an appropriate image analysis software to evaluate the characteristics of the track channels.

The white vertical line in Figure 1c has a width of exactly 10 nm. This is the maximum width of heavy ion tracks in polymers observed with TEM.[14–17] The dark stripes representing Xe ion tracks are approximately three times wider, which acts as evidence that the used preparation technique provides visualization of the outer track region, that is, the halo. This region is not detectable by TEM or SAXS because these methods are sensitive to the gravimetric density when applied to polymers.

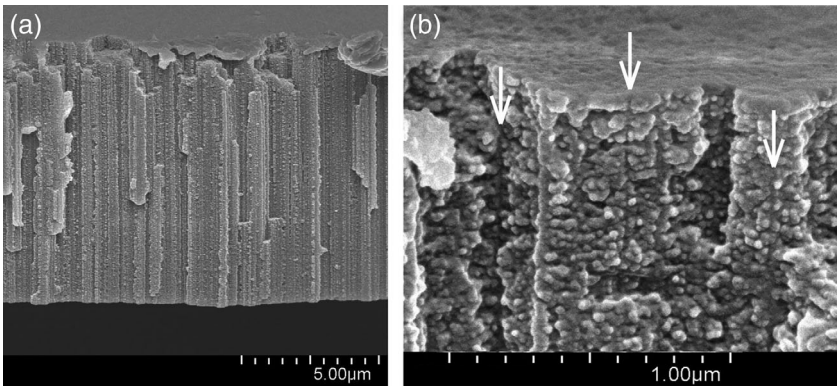


**FIGURE 8** Polypropylene foil irradiated with Au ions at a fluence of $2{\cdot}10^{10}$ $cm^{-2}$. Whole fracture (a) and a fragment at a higher magnification (b). The sample was exposed to nonfiltered UV radiation for 76 h. The white arrows in image (b) point to individual tracks

In the halo, the density of the matrix does not decrease. Instead, in some polymers, the density in this zone may increase due to cross-linking.[18,19] Cross-linking implies formation of additional covalent bonds between macromolecular chains. Therefore, part of intermolecular distances is replaced with shorter intramolecular ones which results in the compaction of the polymer. At the same time, the cross-linked polymer is amorphized because each interchain covalent bond is a structure defect preventing the regular arrangement of segments of neighboring chains. In the case of PET, part of the intermolecular bonds link aromatic rings and create extended π-conjugated structures. Such structures absorb electromagnetic radiation in the UVA range and, therefore, an exposure to the filtered UV light has a preferential impact on the latent track.[9,43] Photooxidation of the above structures leads to a decrease in optical absorption (see Figure 6), an increase in the concentration of carboxylic end groups and the formation of low-molecular products.[9,43]

The compaction of the polymer around the track core may also contribute to the formation of the visible channels on the fractured surfaces. There are examples where the cross-linking is used deliberately to enlarge nanopores via the lateral shrinking of their walls.[44] Similarly, the structures observed at high ion fluences (Figure 1a,b and, probably, Figure 8) could be created at least partially due to the mechanism of anisotropic contraction.

Based on the above discussion, a simple scheme can be suggested to explain the transformations in the ion-irradiated PET under a long UV exposure (Figure 7). The pristine PET consists of amorphous and crystalline domains evenly distributed in the bulk. Ion tracks pierce the polymer foil and create amorphous channels consisting of degraded material (track core) and cross-linked material (track halo). The UV exposure leads to the degradation of the polymer in the amorphous phase including the tracks. Soft UV radiation does not destroy crystallites. Since the typical size of crystalline and amorphous domains in the bulk polymer is smaller than the width of ion tracks, the situation is favorable for their observation.

A less favorable situation occurs if the polymer has a coarser granular structure. Figure 8 shows a fracture of the PP foil irradiated with Au ions. Embrittlement with nonfiltered UV radiation was employed because PP has a low optical absorption both in the UVA and UVB ranges. Due to high ion fluence, the fractured surface has an obvious anisotropic relief (Figure 8a). However, it is difficult to observe individual tracks. Only some of them can reliably be identified (Figure 8b). Crystalline grains in PP have a diameter of 20–40 nm, while the dark channels—the candidates for being the tracks—have a width of approximately 10 nm. Track halos do not appear. A possible reason for this could be the long-range migration of excitations and active radiolysis products in polyolefines—a phenomenon that has been known for a long time both for low-LET irradiation[45] and SHI effects.[46] The ionization and excitation energy that left the track core is dissipated over a large volume and does not create a detectable track halo. Nevertheless, a crosslinked network is readily formed throughout the bulk of a PP sample under SHI bombardment.[46]

## 4 | CONCLUSIONS

To our knowledge, SEM images of latent SHI tracks in the bulk of the material have never been reported before. In this work, we demonstrated that latent tracks of heavy ions with sufficiently large atomic numbers can be captured and viewed on fractured surfaces of semicrystalline polymers. Using controlled photodegradation, the morphology of the polymer can be modified in such a way that ion tracks are visible in a FESEM as structureless channels on a granular background. The dose and the spectrum of UV radiation should be accurately adjusted to obtain a good image. The suggested method is quite specific with regard to the type of polymer. Certain

combinations of morphological, optical and photochemical properties should be fulfilled to achieve a positive result. PET foils—a very important material in the practical context—possess the needed properties. We demonstrated this on two commercial foils of different origins.

In contrast to the TEM technique, the observation of latent tracks in FESEM does not suffer from fast fading. The samples are stable under the electron beam for tens of minutes.

Compared to TEM images of latent ion tracks in PET, those in FESEM have a larger diameter and include both the track core and the outer shell. This result is important with regard to the questions whether this shell exists and whether the properties of the polymer in this zone differ much from the pristine material. The answer to both questions is yes. These features of the SHI tracks may help to better understand the properties of the track-etched nanopores the diameter of which is sometimes smaller than the track diameter. We believe that the approach developed in the work may also be employed in other studies where the synergetic action of ion bombardment and UV irradiation is used to create new functional materials.

## ACKNOWLEDGMENTS

The authors are grateful to the Materials Research group (GSI Helmholtzzentrum für Schwerionenforschung, Darmstadt) for providing samples irradiated with Au ions. The authors thank O. M. Ivanov, N.S. Kirilkin, and N. E. Lizunov for their assistance in experiments. Caren Rossouw's help with proofreading the manuscript is highly appreciated.

## ORCID

*Pavel Y. Apel* https://orcid.org/0000-0003-1259-163X

## REFERENCES

[1] R. L. Clough, *Nucl. Instrum. Meth. Phys. Res. B* **2001**, *185*, 8.
[2] M. Ferry, Y. Ngono-Ravache, C. Aymes-Chodur, M. C. Clochard, X. Coqueret, L. Cortella, E. Pelizzi, S. Rouif, S. Esnouf, Ionizing Radiation Effects in Polymers. in *Reference Module in Materials Science and Materials Engineering* (Ed: S. Hashmi), Elsevier, Oxford **2016**, p. 1.
[3] M. Lang, F. Djurabekova, N. Medvedev, M. Toulemonde, C. Trautmann, *Fundamental Phenomena and Applications of Swift Heavy Ion Irradiations. Comprehensive Nuclear Materials*, 2nd ed., Elsevier, Amsterdam, The Netherlands **2020**.
[4] P. Y. Apel, *Radiat. Phys. Chem.* **2019**, *159*, 25.
[5] N. Betz, *Nucl. Instrum. Meth. in Phys. Res. B* **1995**, *105*, 55.
[6] P. Y. Apel, I. V. Blonskaya, O. L. Orelovitch, B. A. Sartowska, R. Spohr, *Nanotechnology* **2012**, *23*, 225503.
[7] M. Yoshida, Y. Kimura, J. Chen, M. Asano, Y. Maekawa, *Radiat. Phys. Chem.* **2009**, *78*, 1060.
[8] M.-C. Clochard, T. Berthelot, C. Baudin, N. Betz, E. Balanzat, G. Gebel, A. Morin, *J. Power Sources* **2010**, *195*, 223.
[9] P. Wang, M. Wang, F. Liu, S. Ding, X. Wang, G. Du, J. Liu, P. Apel, P. Kluth, C. Trautmann, Y. Wang, *Nat. Commun.* **2018**, *9*, 569.
[10] D. Albrecht, P. Armbruster, R. Spohr, M. Roth, K. Schaupert, H. Stuhrmann, *Appl. Phys. A: Mater. Sci. Process.* **1985**, *37*, 37.
[11] D. Schauries, M. D. Rodriguez, B. Afra, T. Bierschenk, C. Trautmann, S. Mudie, P. Kluth, *Nucl. Instrum. Meth. Phys. Res. B* **2015**, *365*, 573.
[12] S. Abu Saleh, Y. Eyal, *Appl. Phys. Lett.* **2004**, *85*, 2529.
[13] S. Abu Saleh, Y. Eyal, *Nucl. Instrum. Meth. Phys. Res. B* **2005**, *236*, 81.
[14] J. Vetter, G. H. Michler, I. Naumann, *Radiat. Eff. Defects Solids* **1998**, *143*, 273.
[15] Y. Eyal, K. Gassan, *Nucl. Instrum. Meth. Phys. Res. B* **1999**, *156*, 183.
[16] A. Adla, V. Buschmann, H. Fuess, C. Trautmann, *Nucl. Instrum. Meth. Phys. Res. B* **2001**, *185*, 210.
[17] A. Adla, H. Fuess, C. Trautmann, *J. Polym. Sci.: Part B* **2003**, *41*, 2892.
[18] P. Y. Apel, A. Schulz, R. Spohr, C. Trautmann, V. Vutsadakis, *Nucl. Instrum. Meth. Phys. Res. B* **1998**, *146*, 468.
[19] P. Y. Apel, I. V. Blonskaya, V. R. Oganessian, O. L. Orelovitch, C. Trautmann, *Nucl. Instrum. Meth. Phys. Res. B* **2001**, *185*, 216.
[20] P. Y. Apel, P. Ramirez, I. V. Blonskaya, O. L. Orelovich, B. Sartowska, *Phys. Chem. Chem. Phys.* **2014**, *16*, 15214.
[21] N. Rozlosnik, L. Sajo Bohus, C. Birattari, E. Gadioli, L. P. Biro, K. Havancsak, *Nanotechnology* **1997**, *8*, 32.
[22] F. Ohnesorge, R. Neumann, *Europhys. Lett.* **2000**, *50*, 742.
[23] L. S. Farenzena, R. P. Livi, M. A. De Araujo, G. G. Bermudez, R. M. Papaléo, *Phys. Rev. B* **2001**, *63*, 104108.
[24] H. Kudoh, Y. Morita, *J. Polym. Sci. B: Polym. Phys.* **2001**, *39*, 757.
[25] Y. Takeshita, T. Sakurai, A. Asano, K. Takano, M. Omichi, M. Sugimoto, S. Seki, *Adv. Mater. Lett.* **2015**, *6*, 99.
[26] A. Z. Tuleushev, M. V. Zdorovets, A. L. Kozlovskiy, F. E. Harrison, *Crystals* **2020**, *10*, 427.
[27] I. Karacan, A. K. Taraiya, D. I. Bower, I. M. Ward, *Polymer* **1993**, *34*, 2691.
[28] J. F. Ziegler, J. P. Biersack, U. Littmark, *The Stopping and Range of Ions in Solids*, Pergamon, New York **1985**.
[29] K. C. Cole, A. Ajji, E. Pellerin, *Macromolecules* **2002**, *35*, 770.
[30] H. Chang, J. M. Schultz, R. M. Gohil, *J. Macromol. Sci. B* **1993**, *32*, 99.
[31] F. Dinelli, H. E. Assender, K. Kirov, O. V. Kolosov, *Polymer* **2000**, *41*, 4285.
[32] E. Wohlfart, J. P. Fernandez-Blazquez, E. Knoche, A. Bello, E. Perez, E. Arzt, A. del Campo, *Macromolecules* **2010**, *43*, 9908.
[33] K. Teshima, H. Sugimura, Y. Inoue, O. Takai, A. Takano, *Langmuir* **2003**, *19*, 10624.
[34] T. Steckenreiter, E. Balanzat, H. Fuess, C. Trautmann, *Nucl. Instrum. Meth. Phys. Res. B* **1997**, *131*, 159.
[35] C. Liu, Y. Jin, Z. Zhu, Y. Sun, M. Hou, Z. Wang, Y. Wang, C. Zhang, X. Chen, J. Liu, B. Li, *Nucl. Instrum. Meth. Phys. Res. B* **2000**, *169*, 72.
[36] M. Djebara, J. P. Stoquert, M. Abdesselam, D. Muller, A. C. Chami, *Nucl. Instrum. Meth. Phys. Res. B* **2012**, *274*, 70.
[37] M. Day, D. M. Wiles, *J. Appl. Polym. Sci.* **1972**, *16*, 191.
[38] J. Verdu, *J. Macromol. Sci. A* **1994**, *31*, 1383.

[39] A. Polyakova, E. V. Stepanov, D. Sekelik, D. A. Schiraldi, A. Hiltner, *J. Polym. Sci. B: Polym. Phys.* **2001**, *39*, 1911.
[40] J. Lin, S. Shenogin, S. Nazarenko, *Polymer* **2002**, *43*, 4733.
[41] S. S. Fernando, P. A. Christensen, T. A. Egerton, J. R. White, *Polym. Degrad. Stab.* **2009**, *94*, 83.
[42] D. C. Miles, J. H. Briston, *Polymer Technology*, 3rd ed., Chemical Publishing Co., New York **1996**.
[43] P. Y. Apel, I. V. Blonskaya, O. M. Ivanov, O. V. Kristavchuk, N. E. Lizunov, A. N. Nechaev, O. L. Orelovich, O. A. Polezhaeva, S. N. Dmitriev, *Membr. Membr. Technol.* **2020**, *2*, 98.
[44] U. Jeong, D. Y. Ryu, J. K. Kim, D. H. Kim, T. P. Russell, C. J. Hawker, *Adv. Mater.* **2003**, *15*, 1247.
[45] G. Ungar, *J. Mater. Sci.* **1981**, *16*, 2635.
[46] P. Y. Apel, A. Y. Didyk, A. G. Salina, *Nucl. Instrum. Meth. Phys. Res. B* **1996**, *107*, 276.

**How to cite this article:** Blonskaya IV, Kristavchuk OV, Nechaev AN, Orelovich OL, Polezhaeva OA, Apel PY. Observation of latent ion tracks in semicrystalline polymers by scanning electron microscopy. *J Appl Polym Sci*. 2020; e49869. https://doi.org/10.1002/app.49869